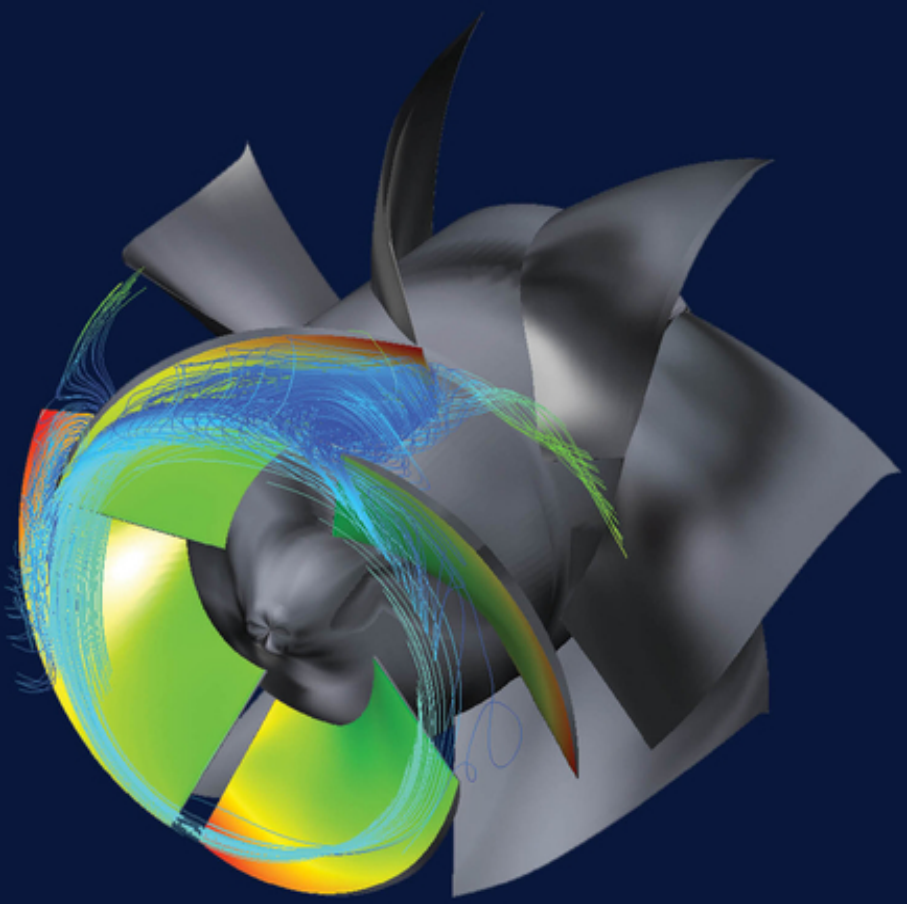

Mixed-flow Pumps

Modeling, Simulation, and Measurements

Wei Li, Leilei Ji, Ramesh Agarwal,
Weidong Shi, Ling Zhou

ASME PRESS

WILEY

Mixed-flow Pumps

Wiley-ASME Press Series

Thermal Spreading and Contact Resistance: Fundamentals and Applications
Yuri S. Muzychka and M. Michael Yovanovich

Analysis of ASME Boiler, Pressure Vessel, and Nuclear Components in the Creep Range
Maan H. Jawad and Robert I. Jetter

Voltage-Enhanced Processing of Biomass and Biochar
Gerardo Diaz

Pressure Oscillation in Biomedical Diagnostics and Therapy
Ahmed Al-Jumaily and LuluWang

Robust Control: Youla Parameterization Method
Farhad Assadian and Kevin R. Mellon

Metrology and Instrumentation: Practical Applications for Engineering and Manufacturing
Samir Mekid

Fabrication of Process Equipment
Owen Greulich and Maan H. Jawad

Engineering Practice with Oilfield and Drilling Applications
DonaldW. Dareing

Flow-Induced Vibration Handbook for Nuclear and Process Equipment
Michel J. Pettigrew, Colette E. Taylor, and Nigel J. Fisher

Vibrations of Linear Piezostructures
Andrew J. Kurdila and Pablo A. Tarazaga

Bearing Dynamic Coefficients in Rotordynamics: Computation Methods and Practical Applications
Lukasz Brenkacz

Advanced Multifunctional Lightweight Aerostructures: Design, Development, and Implementation
Kamran Behdinan and Rasool Moradi-Dastjerdi

Vibration Assisted Machining: Theory, Modelling and Applications
Li-Rong Zheng, Dr. Wanqun Chen, and Dehong Huo

Two-Phase Heat Transfer
Mirza Mohammed Shah

Computer Vision for Structural Dynamics and Health Monitoring
Dongming Feng and Maria Q Feng

Theory of Solid-Propellant Nonsteady Combustion
Vasily B. Novozhilov and Boris V. Novozhilov

Introduction to Plastics Engineering
Vijay K. Stokes

Fundamentals of Heat Engines: Reciprocating and Gas Turbine Internal Combustion Engines
Jamil Ghojel

Offshore Compliant Platforms: Analysis, Design, and Experimental Studies
Srinivasan Chandrasekara and R. Nagavinothini

Computer Aided Design and Manufacturing
Zhuming Bi and Xiaoqin Wang

Pumps and Compressors
Marc Borremans

Corrosion and Materials in Hydrocarbon Production: A Compendium of Operational and Engineering Aspects
Bijan Kermani and Don Harrop

Design and Analysis of Centrifugal Compressors
Rene Van den Braembussche

Case Studies in Fluid Mechanics with Sensitivities to Governing Variables
M. Kemal Atesmen

The Monte Carlo Ray-Trace Method in Radiation Heat Transfer and Applied Optics
J. Robert Mahan

Dynamics of Particles and Rigid Bodies: A Self-Learning Approach
Mohammed F. Daqaq

Primer on Engineering Standards, Expanded Textbook Edition
Maan H. Jawad and Owen R. Greulich

Engineering Optimization: Applications, Methods and Analysis
R. Russell Rhinehart

Compact Heat Exchangers: Analysis, Design and Optimization using FEM and CFD Approach
C. Ranganayakulu and Kankanhalli N. Seetharamu

Robust Adaptive Control for Fractional-Order Systems with Disturbance and Saturation
Mou Chen, Shuyi Shao, and Peng Shi

Robot Manipulator Redundancy Resolution
Yunong Zhang and Long Jin

Stress in ASME Pressure Vessels, Boilers, and Nuclear Components
Maan H. Jawad

Combined Cooling, Heating, and Power Systems: Modeling, Optimization, and Operation
Yang Shi, Mingxi Liu, and Fang

Applications of Mathematical Heat Transfer and Fluid Flow Models in Engineering and Medicine
Abram S. Dorfman

Bioprocessing Piping and Equipment Design: A Companion Guide for the ASME BPE Standard
William M. (Bill) Huitt

Nonlinear Regression Modeling for Engineering Applications: Modeling, Model Validation, and Enabling Design of Experiments
R. Russell Rhinehart

Geothermal Heat Pump and Heat Engine Systems: Theory and Practice
Andrew D. Chiasson

Fundamentals of Mechanical Vibrations
Liang-Wu Cai

Introduction to Dynamics and Control in Mechanical Engineering Systems
Cho W.S. To

Thermal Spreading and Contact Resistance: Fundamentals and Applications
Yuri S. Muzychka and M. Michael Yovanovich

Mixed-flow Pumps: Modeling, Simulation, and Measurements
Wei Li, Leilei Ji, Ramesh Agarwal, Weidong Shi, and Ling Zhou

This Work is a co-publication between John Wiley & Sons, Inc. and ASME Press.

Mixed-flow Pumps

Modeling, Simulation, and Measurements

Wei Li
Jiangsu University, China

Leilei Ji
Jiangsu University, China

Ramesh Agarwal
Washington University in St. Louis, USA

Weidong Shi
Nantong University, China

Ling Zhou
Jiangsu University, China

ASME PRESS

WILEY

This Work is a co-publication between John Wiley & Sons, Inc. and ASME Press.
Published simultaneously in Canada.

Library of Congress Cataloging-in-Publication Data:

Names: Li, Wei (Professor of engineering), author. | Ji, Leilei, author. | Agarwal, R. K. (Ramesh K.), author. | Shi, Weidong (College presidents), author. | Zhou, Ling (Professor), author.
Title: Mixed-flow pumps : modeling, simulation, and measurements / Wei Li, Leilei Ji, Ramesh Agarwal, Weidong Shi, Ling Zhou.
Description: Hoboken, NJ : Wiley, [2024] | Series: Wiley-ASME press series | Includes index.
Identifiers: LCCN 2024009766 (print) | LCCN 2024009767 (ebook) | ISBN 9781119910787 (hardback) | ISBN 9781119910794 (adobe pdf) | ISBN 9781119910374 (epub)
Subjects: LCSH: Centrifugal pumps. | Computational fluid dynamics.
Classification: LCC TJ919 .L38 2024 (print) | LCC TJ919 (ebook) | DDC 621.6/7–dc23/eng/20240319
LC record available at https://lccn.loc.gov/2024009766
LC ebook record available at https://lccn.loc.gov/2024009767

Cover Design: Wiley
Cover Image: Courtesy of Wei Li, Leilei Ji, Ramesh Agarwal, Weidong Shi, Ling Zhou

Set in 9.5/12.5pt STIXTwoText by Straive, Chennai, India

Contents

Preface *xi*
Acknowledgments *xiii*
List of Acronyms *xv*
List of Symbols *xvii*

1 Introduction *1*
1.1 What Is a Mixed-flow Pump? *1*
1.2 Types of Mixed-flow Pumps *1*
1.3 Agricultural and Industrial Applications of Pumps *2*
1.4 Summary *4*
References *5*

2 Basic Concepts and Theory of Mixed-flow Pumps *7*
2.1 Basic Flow and Performance Parameters *7*
2.1.1 Volume Flow Q *7*
2.1.2 Head H *7*
2.1.3 Speed n *8*
2.1.4 *NPSH* *8*
2.1.5 Power and Efficiency *8*
2.2 Typical Type of Flows in the Mixed-flow Pumps *9*
2.2.1 Tip Leakage Flow *9*
2.2.2 Rotating Stall *10*
2.2.3 Cavitation Flow *12*
2.3 Summary *15*
Nomenclature *15*
References *15*

3 Brief Review of Computational Fluid Dynamics *21*
3.1 CFD as a Flow Simulation Tool *21*
3.2 Geometry Modeling *24*
3.3 Mesh Generation *24*
3.4 Governing Equations of Fluid Dynamics *25*
3.5 Simulation of Turbulent Flows *25*
3.6 Turbulence Modeling *28*
3.6.1 Standard $k-\varepsilon$ Model *28*

3.6.2 Shear Stress Transport (SST) $k-\omega$ Model *29*
3.6.3 Spalart–Allmaras (SA) Model *32*
3.6.4 Wray–Agarwal (WA) Model *33*
3.6.5 Detached Eddy Simulation Model *34*
3.6.6 Large Eddy Simulation (LES) Model *35*
3.7 Numerical Solution Algorithms *37*
3.7.1 Numerical Discretization Method *37*
3.7.2 Flow Field Solution Method *38*
3.8 Near-wall Flow Treatment *38*
3.9 Boundary Conditions *40*
3.10 Uncertainty Analysis *41*
3.11 Summary *43*
Nomenclature *44*
References *44*

4 Pump Performance Analysis Methods *47*
4.1 Entropy Production Analysis *47*
4.2 Vortex Identification and Vorticity Transport *49*
4.2.1 Vortex Identification *49*
4.2.1.1 Q-Criterion *49*
4.2.1.2 Regularized Helicity Method *50*
4.2.2 Vorticity Transport *50*
4.3 Transient Flow Analysis Using the Wavelet Method *51*
4.4 Summary *54*
References *54*

5 Experimental Methods, Data, and Analysis *57*
5.1 External Characteristics Experiment *57*
5.1.1 Test Equipment and Instruments *57*
5.1.2 Test Method for External Flow Characteristics of the Pump *60*
5.1.3 Uncertainty Analysis of the Experiment *61*
5.1.4 Test Results for External Flow Characteristics of the Pump *62*
5.2 Experiment for Measuring Pressure Fluctuations *64*
5.2.1 Experimental Procedure *65*
5.2.2 Wavelet Transform of Pressure Pulsation for Different Tip Clearances *68*
5.2.3 Coherence of Pressure Pulsation for Different Tip Clearances *72*
5.3 PIV Measurement *75*
5.3.1 Basic Principles of PIV Measurement *75*
5.3.2 The PIV Image Processing System *76*
5.3.3 PIV Measurement Criteria *77*
5.3.4 PIV Testing Instruments and System *77*
5.3.5 PIV Test Method *79*
5.3.5.1 Selection and Addition of Tracer Particles *79*
5.3.5.2 Calibration Apparatus *79*
5.3.5.3 Lens Group, Camera Fixing, and Adjustment *79*
5.3.5.4 Shooting Section of the Dynamic and Static Interference Flow Field *82*
5.3.5.5 Positions of the Equipment and the Shooting Sections *83*

5.3.6 Analysis of the PIV Results for the Flow Field of the Front Shaft Section of the Impeller Inlet *84*
5.3.7 Relative Velocity Distribution at the Monitoring Lines in Different Phases at the Impeller Inlet and Outlet Under the Part-loading Conditions *92*
5.4 Orbit of Shaft Centerline *95*
5.4.1 Measurement of the Spindle Axis Trajectory *95*
5.4.2 Characteristics of Vibrations of the Shaft System *97*
5.4.3 Original Axis Trajectory Diagram and Time-domain Diagram *98*
5.4.4 Decomposition and Refinement of the Rotor Axis-centered Trajectory *100*
5.4.5 Flow Spectrum Analysis *101*
5.4.6 Effect of the Rotor–Stator Interaction on the Shaft Vibration *103*
5.5 Summary *104*
References *105*

6 CFD Simulations of a Mixed-flow Pump Using Various Turbulence Models *107*
6.1 Comparison and Validation of Numerical Results from Three Two-equation Turbulence Models (SST k–ω, k–ω, and Standard k–ε) *107*
6.1.1 Comparison of Energy Performance *107*
6.1.2 Comparison of CFD Results with Phase-Averaged Velocity Predictions from PIV *107*
6.1.3 Flow Field Under Incipient Stall Condition *111*
6.2 Application of Wray–Agarwal (WA) One-Equation Turbulence Model *116*
6.2.1 Energy Performance Comparison *117*
6.2.2 Comparison of the Flow Field in the Rotor–Stator Interaction Zone Using Different Turbulence Models *118*
6.2.3 Comparison of Eddy Viscosity Variable $R = k/\omega$ in the Pump Using the Four Turbulence Models (SST k–ω, k–ω, k–ε, and WA) *119*
6.3 Summary *123*
References *124*

7 Tip Leakage Flow In a Mixed-flow Pump *125*
7.1 Energy Characteristics *125*
7.1.1 Comparison of Energy Performance of the Pump for Various Tip Clearances *125*
7.1.2 Distribution of the Total Entropy Production in the Pump for Various Tip Clearances *126*
7.1.3 Local Entropy Production Rate in the Impeller *130*
7.1.4 Local Entropy Production Rate in the Guide Vane *133*
7.2 Flow Structures *135*
7.2.1 Vortex Patterns in the Blade Rim Region of the Pump for Various Tip Clearances *135*
7.2.2 Tip Leakage Vortex (TLV) Intensity and the Vortex Core Distribution *136*
7.3 Unsteady Flow Characteristics *138*
7.3.1 Time-domain Analysis of the Pressure Pulsations *138*
7.3.2 Frequency-domain Analysis of the Pressure Pulsation *139*
7.4 Transient Flow Field Due to Rotor–Stator Interaction (RSI) *140*
7.4.1 Flow Fields Before the RSI Zone *140*
7.4.2 Flow Fields in the RSI Zone *140*
7.4.3 Pressure Fluctuation in Partial-loading Conditions *145*

7.4.3.1 Time-domain Analysis *145*
7.4.3.2 Frequency-domain Analysis *147*
7.5 Summary *151*
References *152*

8 Rotational Stall in a Mixed-flow Pump *153*
8.1 Energy Characteristics *153*
8.1.1 Energy Performance of the Pump Along the Axial Flow Direction *153*
8.1.2 Energy Loss Mechanism Under Stall Condition *153*
8.1.2.1 Theoretical Analysis of Head Drop in Saddle Area *153*
8.1.2.2 Flow Distribution in Each Channel *155*
8.1.2.3 Region of the Maximum Energy Loss in the Impeller *157*
8.2 Flow Structure in the Critical and Deep Stall Conditions *158*
8.2.1 Flow Structure in the Impeller in the Design, Critical, and Deep Stall Conditions *158*
8.2.2 Key Factors Causing the Energy Loss *160*
8.2.2.1 Influence of the Inlet Swirl on Energy Loss *160*
8.2.2.2 Influence of the Tip Leakage Vortex on the Energy Loss *162*
8.2.2.3 Influence of the Stall Vortex on the Energy Loss *166*
8.2.2.4 Influence of the Backflow Vortex on the Energy Loss *168*
8.3 Effect of the Tip Clearance on the Rotating Stall *170*
8.3.1 TLF Patterns and TLV Core Trajectories for Different Tip Clearances *170*
8.3.2 Influence of the Inlet Swirl Flow and the TLV Characteristics *175*
8.3.3 Distorted Flow in the Blade Rim Region Below the TLV *175*
8.4 Propagation Characteristics of Rotating Stall *179*
8.4.1 Pressure Fluctuation Characteristics of the Flow in the Stall Condition *179*
8.4.2 Correlation Between the Transient Flow Field and the Energy Characteristics of the Pump *182*
8.4.3 Morphology and Propagation Mechanism of Rotating Stall *186*
8.5 Inducements for the Circumferential Propagation of the Rotating Stall *189*
8.6 A Stall Prediction Model of the Mixed-flow Pump *191*
8.6.1 Flow Characteristics During the Process of the Stall for Impellers with Different Blade Numbers *191*
8.6.2 Quantitative Analysis of the Suction Surface Parameters of the Stalled Blades *194*
8.6.3 The Pressure and Velocity Distributions on the Suction Side of the Blade of the Impellers with Various Blade Numbers *198*
8.6.4 A Simple Stall Prediction Model *198*
8.7 Summary *202*
References *203*

9 Passive Suppression of Rotating Stall in Mixed-flow Pump *205*
9.1 Introduction *205*
9.2 Impeller Blade Rim Structures for Stall Suppression *207*
9.2.1 Geometries of Various Blade Rim Structures *207*
9.2.2 Results of Numerical Calculations for Various Blade Rim Structures *208*
9.2.2.1 Comparison of the External Characteristics of the Pump for Various Blade Rim Structures *208*
9.2.2.2 Influence of Blade Rim Geometry on the Flow Field in Rim Clearance Region *210*

9.2.2.3 Influence of Blade Rim Structure on the Inlet Flow Angle of the Impeller *212*
9.2.2.4 Distribution of Vortex Structures in the Impeller with Different Rim Structures *220*
9.3 Influence of the Circumferential Spokes *227*
9.3.1 The Structure of "O-Spoke" *227*
9.3.2 Analysis of Results *228*
9.3.2.1 External Characteristics Analysis *228*
9.3.2.2 Analysis of the Flow Field in Various Cross-Sectional Areas of the Pump *230*
9.3.2.3 Flow Field Analysis in the Impeller Shroud Region *232*
9.3.2.4 Energy Performance Analysis Based on the Entropy Generation Theory *235*
9.3.2.5 Analysis of the Blade Height Section Flow Field *235*
9.4 Summary *237*
References *238*

10 Cavitation in a Mixed-flow Pump *241*
10.1 Numerical Model *241*
10.1.1 Cavitation Model *241*
10.1.2 Numerical Simulation Setup and Boundary Conditions *242*
10.1.3 Cavitation Test Procedure *242*
10.1.4 Comparison of Numerical Simulations and Cavitation Test Results *243*
10.2 Flow Characteristics of the Mixed-flow Pump Under Cavitation *245*
10.2.1 Blade Surface Load Distribution *245*
10.2.2 Trajectory of TLV for Different Values of $NPSH_a$ *247*
10.2.3 Evolution of the Transient Flow Trajectory of the TLV and Tip Cavitation Flow *247*
10.3 Analysis of Cavitation Energy Characteristics *251*
10.3.1 Analysis of Pump Energy Characteristics *251*
10.3.2 Analysis of Energy Loss in the End Wall Region of the Pump Caused by the TLV-Induced Cavitation *251*
10.3.3 Effect of Cavitation on the Output Power of the Pump *253*
10.3.4 Effect of Cavitation on Energy Losses in the Pump *255*
10.4 Summary *257*
References *258*

11 Analysis of the Vortex Dynamics Characteristics in the Tip Region of the Mixed-flow Pump Under Cavitation *259*
11.1 The Tip Leakage Flow Characteristics Under Cavitation *259*
11.1.1 Tip Leakage Flow Characteristics *259*
11.1.2 Evolution of the Vorticity and Its Intensity *262*
11.1.3 Turbulent Kinetic Energy Distribution in the Blade Tip Region *264*
11.2 Analysis of the Vorticity Transport Characteristics in the Tip Region *268*
11.2.1 Radial Vorticity Transport in the Cavitation Region Near the Blade Tip *268*
11.2.2 Circumferential Transport of Vorticity *272*
11.2.3 Transport of the Axial Vorticity *273*
11.2.4 Quantitative Evaluation of the Vorticity Transport Terms *276*
11.3 Summary *281*
References *282*

12 Multiphase Flow Simulations of Sediment Particles in Mixed-flow Pumps *283*
12.1 Introduction *283*
12.2 Governing Equations of the Mixture Model of Multiphase Flow *285*
12.3 Pump Model and Mesh Generation *286*
12.4 Two-phase Flow Characteristics of the Solid–Liquid Flow in Mixed-flow Pumps *287*
12.4.1 Influence of the Solid Particles on the Energy Characteristics of the Mixed-flow Pumps *287*
12.4.1.1 Influence of the Solid Particles on the Pump Head and Efficiency in Various Flow Conditions *287*
12.4.1.2 Influence of Different Volume Fractions of Solid Phase on the Pump Head and Efficiency *287*
12.4.2 Distribution of the Solid Phase Inside the Impeller of the Pump *289*
12.4.3 Analysis of the Energy Loss in the Mixed-flow Pump *291*
12.4.4 Analysis of the Energy Loss Inside the Impeller *293*
12.5 Two-phase Flow Characteristics in the Guide Vane of Mixed-flow Pumps *299*
12.5.1 Distribution of Solid Particles in the Guide Vane of a Mixed-flow Pump *299*
12.5.2 Analysis of the Energy Loss in the Guide Vane *301*
12.6 Summary *304*
References *304*

Index *307*

Preface

Pumps are among the most power-consuming general-purpose equipment in energy conversion devices and significantly impact the modern industrial economy. A mixed-flow pump can be considered a type of pump design between centrifugal pump and axial flow pump since it employs the combined effect of centrifugal force and thrust generated by the rotation of the impeller to convey fluid, and the fluid flows axially in and diagonally out through the impeller. It can also be called oblique flow pump with high flow rate, high efficiency, strong anti-cavitation performance, etc. It is widely used for agricultural irrigation, municipal water supply and drainage, water circulation in power industry, naval water jet propulsion, underwater weapon launches, and regional water transfer projects.

Compared to other pump types, the internal flow of mixed-flow pumps is more complex, and the secondary flow and deliquescence are more prominent. There are not only inherent unsteady flow problems caused by the static and dynamic interference but also unsteady problems induced by the wheel edge leakage vortex and its trailing off, rotational stall, and other complex flow phenomena which seriously affect the operational stability and efficiency of the mixed-flow pumps. Therefore, there is a need to explore the spatial and temporal evolution of flow structures and flow dynamics of the internal flow field of a mixed-flow pump as well as to achieve the desired targeted optimized solutions. In addition, the internal vortex energy loss characteristics of mixed-flow pumps, cavitation damage, and other phenomena also need to be studied systematically. Understanding and mastering the physical mechanisms of the internal flow in a mixed-flow pump is a prerequisite for improving the operational stability, reliability, and efficiency of the pump.

In previous studies, the flow field and performance characteristics of a mixed-flow pump were generally determined and analyzed by experimental means; however, the experimental approach is not only expensive, but it is often difficult to observe and obtain all the details of the flow field experimentally due to its complex structure. In recent years, the emergence of computational fluid dynamics has provided an effective tool to study the finer details of the flow structure inside the hydraulic machinery, which is uniquely beneficial in analyzing the internal flow field in a mixed-flow pump at multiple scales for a full range of operating conditions. Currently, there are no reference books providing the computational approach for the study of the flow fields and performance of mixed-flow pumps. Therefore, this book selects a typical model of a guide vane-type mixed-flow pump as the object of study and systematically investigates the complex internal flow structure through numerical simulations and experiments aiming to provide a reference work for industrial practitioners, academics, and students interested in the field of hydraulic machinery.

The book is divided into 12 chapters; the content of each chapter is as follows.

The first chapter provides a brief introduction to the definitions, types, and applications of mixed-flow pumps. The second chapter provides a detailed description of the basic concepts of mixed-flow pumps and the related theories. Chapter 3 focuses on computational fluid dynamics (CFD) simulation technology including geometric modeling, meshing, governing equations of fluid flow, CFD methods classification, turbulence models, solution algorithms, near-wall surface treatment, and boundary conditions. Chapter 4 describes different analysis methods including entropy production analysis, vortex analysis, and wavelet methods. Chapter 5 details the experimental methods, data, and analysis such as pressure pulsation measurements, PIV measurements, and axial trajectory measurements. Chapter 6 covers the application of turbulence models and compares the applicability of several turbulence models in the performance prediction of mixed-flow pumps. Chapter 7 investigates and analyzes the energy characteristics, flow structure, instability characteristics, and dynamic and static interference of the tip leakage flow of the mixed-flow pump. Chapter 8 investigates and analyzes the energy characteristics, flow structure, and the effect of tip clearance on the rotational stall and its propagation characteristics as well as the causes of incipient and deep rotational stall in the mixed-flow pump. Chapter 9 provides several passive suppression techniques to control the rotating stall in the mixed-flow pump. Chapter 10 analyzes the cavitation flow field and cavitation energy characteristics of the mixed-flow pump. Chapter 11 describes a special application of the Wray–Agarwal (WA) one-equation turbulence model to analyze the vortex dynamics characteristics in the tip region of the mixed-flow pump to demonstrate the accuracy and efficiency of the WA model for computing such complex flows compared to the other widely used turbulence models. Chapter 12 investigates the influence of the sediment particles on internal energy dissipation of the mixed-flow pump with different solid-phase volume fractions.

This book has been limited in terms of the depth and breadth of data collection. Furthermore, there could inevitably be some shortcomings and errors in the book. We hope that readers will provide comments and input so that future editions can be improved.

Acknowledgments

This work was sponsored by the Key International Cooperative Research Program of the National Natural Science Foundation of China (No. 52120105010), the National Key R&D Project (No. 2020YFC1512405) of China, the National Natural Science Foundation of China (No. 52179085 and No. 52309112), the Sixth "333 High Level Talented Person Cultivating Project" of Jiangsu Province, projects of the "Blue Project" in Jiangsu Colleges and Universities, and China Postdoctoral Science Foundation (No. 2022TQ0127 and No. 2023M741414); Open Research Subject of Key Laboratory of Fluid and Power Machinery (Xihua University), Ministry of Education (LTDL-2022010).

The publication of this book was made possible by the help of several colleagues and students at the National Engineering Research Center for Pumps and Systems of Jiangsu University and the CFD Laboratory of Washington University in St. Louis, USA, to whom the authors would like to express their sincere gratitude.

In particular, special thanks go to Mingjiang Liu, Shuo Li, Yi Yang, Shenglei He, and others from Jiangsu University for completing the translation of part of this book from Chinese.

The authors would like to dedicate this book to their respective families for their unwavering support, perseverance, and encouragement during the preparation of this book.

List of Acronyms

BPF	blade-passing frequency
BV	bounded vortex
CFD	computational fluid dynamics
CFL	Courant–Fredrick–Levy
DES	detached Eddy simulation
DNS	direct numerical simulation
FFT	fast Fourier transform
GCI	grid convergence index
HRN	high Reynolds number
LE	leading edge
LES	large eddy simulation
LNG	liquefied natural gas
LRN	low Reynolds number
LVC	local vortical cavitation
PDE	partial differential equation
PIV	particle image velocimetry
PS	pressure side
PTLV	primary tip leakage vortex
PV	passage vortex
RANS	Reynolds-averaged Navier-Stokes
RHD	right-hand side
RSI	rotor-stator interaction
RSM	Reynolds stress model
SA	Spalart–Allmaras
SGS	subgrid-scale
SIMPLE	semi-implicit method for pressure-linked equations
SS	suction side
SST	shear stress transport
STLV	secondary tip leakage vortex
SV	secondary vortex
TCC	tip clearance cavitation
TE	trailing edge
TLF	tip leakage flow

TLV	tip leakage vortex
TLVC	tip leakage vortex core
TMR	turbulence modeling resource
WA	Wray–Agarwal
WTC	wavelet transforms coherence

List of Symbols

Nomenclature

b_2	the width of the impeller, mm
C_p	pressure pulsation coefficient
D_1	the inlet diameter of the impeller, mm
D_2	the outlet diameter of the impeller, mm
D_3	the inlet diameter of the guide vane, mm
D_4	the outlet diameter of the guide vane, mm
D_ω	the cross-diffusion term in turbulence models
G_b	generation of turbulence due to buoyancy in turbulence models
G_k	generation of turbulent kinetic energy due to the mean velocity gradients in turbulence models
G_ω	production term of the turbulent dissipation rate in turbulence models
$h_{\Delta p}$	head drop loss coefficient
H	head, m
H_t	theoretical head, m
i, j	stands for the x, y, z direction
k	turbulent kinetic energy, m^2/s^2
M_t	turbulent Mach number in turbulence models
m_{ji}	time-averaged viscous stress tensor
$\dot{m}$	mass discharge from each domain of the pump, kg/s
$NPSH$	net positive suction head, m
$NPSH_a$	net inlet pressure available, m
$NPSH_r$	net inlet pressure required, m
n	rated speed of the impeller, r/min
n_s	specific speed
p_1, p_2	total pressure at the inlet and outlet of each domain, Pa
P_e	effective power, W
P_{tol}	total input power, W
q	heat flux, J/s
Q	flow rate, m^3/h
Q_{des}	designed flow rate, m^3/h
$\dot{Q}$	energy transfer rate
R	the cross-diffusion term in WA model ($= k/\omega$)
$R(a,b)$	the coherence coefficient

S	strain rate, smoothing operator, standard deviation
s	specific entropy, J/(kg K)
$\dot{S}_D'''$	local entropy production rate, kW/m^3/K^3
$\dot{S}_{\overline{D}}'''$	entropy production rate induced by time-averaged movement, kW/m^3/K^3
$\dot{S}_{D'}'''$	entropy production rate induced by velocity fluctuation, kW/m^3/K^3
t	time, s
T	temperature, K
u	velocity, m/s
u_j	stands for the velocity in different coordinate directions
x	coordinate, m
x_j	stands for the coordinate directions
Y_M	the effect of the expansion of compressible turbulence on the total dissipation rate in turbulence models
Y_k, Y_ω	the dissipation terms of k and ω in turbulence models
y	the distance from the wall
Z	number of impeller blades
Z_d	number of guide vane blades
α_3	average inlet blade angle of guide vane, °
α_4	average outlet blade angle of guide vane, °
β	the coefficient of thermal expansion
β_1	average inlet blade angle of the impeller, °
β_2	average outlet blade angle of the impeller, °
Γ_k, Γ_ω	the coefficients of diffusion term for k and ω in turbulence models
δ_{ij}	Kronecker delta symbol
ε	turbulent dissipation rate, m^2/s^3 in turbulence models
η	efficiency of mixed-flow pump, %
μ	dynamic viscosity, Pa s
μ_t	turbulent viscosity, m^2/s
ρ	density, kg/m^3
σ_k, σ_ε	turbulent Prandtl numbers for k and ε in turbulence models
ϕ	scalar variable
ω	turbulent eddy frequency, s^{-1} in turbulent models

1

Introduction

1.1 What Is a Mixed-flow Pump?

A mixed-flow pump is a centrifugal pump with a mixed-flow impeller [1]. The specific speed (n_s) lies between 35 and 80 rpm for low-speed mixed-flow pumps and between 80 and 160 rpm for higher-speed mixed-flow pumps (in special cases, even higher). It has characteristics of both radial flow and axial flow pumps. As liquid flows through the impeller of a mixed-flow pump, the impeller blades push the liquid out away from the pump shaft and to the pump suction at an angle greater than 90°. The impeller of a typical mixed-flow pump and the flow through a mixed-flow pump are shown in Fig. 1.1.

1.2 Types of Mixed-flow Pumps

Based on the type of suction chamber, mixed-flow pumps can be divided into two types: volute mixed-flow pumps and guide vane mixed-flow pumps, as shown in Fig. 1.2. The former is close to the design of a centrifugal pump, and the latter is close to the design of an axial flow pump.

At present, majority of mixed-flow pumps are volute mixed-flow pumps which are similar to a single-suction centrifugal pump but are different in the type of impeller: the impeller of a mixed-flow pump of high specific speed is similar to that of an axial flow pump which is open type with adjustable blades; the impeller of a mixed-flow pump of low specific speed, on the other hand, is closed type which is similar to that of a single-suction centrifugal pump, but its flow channel is wider and the blade outlet is inclined.

Compared to the axial flow pump, the guide vane mixed-flow pump has slightly higher efficiency and a relatively flat efficiency characteristic curve. In other words, it can ensure higher efficiency when the water level changes; hence, it is very suitable for farmland drainage and irrigation and saves power, but compared to the volute mixed-flow pump, its diameter is smaller. For the vertical guide vane mixed-flow pump, the impeller is submerged in water during operation, so there is no need for water diversion equipment, and therefore the needed floor area is small. Therefore, in places where the axial flow pump is used (except for the axial flow pump with large adjustable blades), it is advantageous to replace it with an appropriate model of guide vane mixed-flow pump.

Other classifications of mixed-flow pumps are:

1. According to the inspection and disassembly form, they can be divided into the extractable mixed-flow pump and the non-extractable mixed-flow pump.
2. According to the blade regulation type, they can be divided into the fixed mixed-flow pump, the semi-regulated submersible axial flow pump, and the fully regulated mixed-flow pump.

Mixed-flow Pumps: Modeling, Simulation, and Measurements, First Edition.
Wei Li, Leilei Ji, Ramesh Agarwal, Weidong Shi, and Ling Zhou.

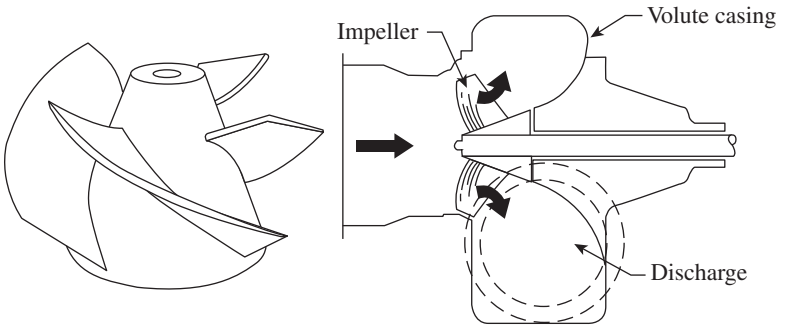

Figure 1.1 Mixed-flow pump impeller and mixed-flow pump model.

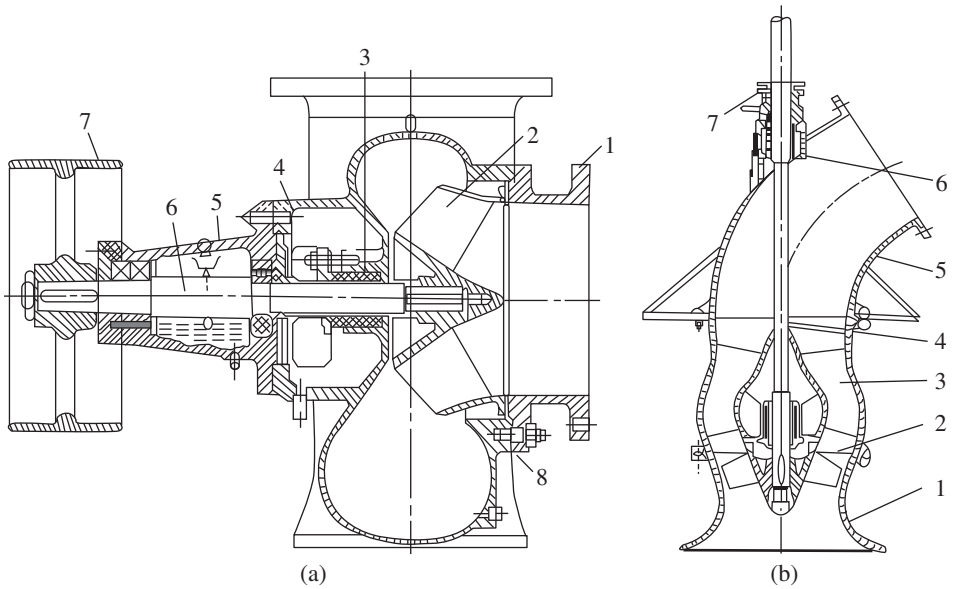

Figure 1.2 Classification of mixed-flow pumps. (a) Structural diagram of volute mixed-flow pump 1. Pump cover, 2. Impeller, 3. Packing, 4. Pump body, 5. Bearing body, 6. Pump shaft, 7. Pulley, 8. Bolt. (b) Structural diagram of guide vane mixed-flow pump. 1. Suction horn, 2. Impeller, 3. Guide vane, 4. Outlet elbow, 5. Pump shaft, 6. Rubber bearing, 7. Stuffing box.

1.3 Agricultural and Industrial Applications of Pumps

Due to the characteristics of moderate head and large flow rate, the mixed-flow pump is widely used in farmland irrigation, flood prevention and drainage, sewage treatment, power station cooling systems, and other applications.

In agricultural production, the main function of the mixed-flow pump is irrigation and drainage. There are vast rural areas in the world, thus a large number of pumps are needed every year. Generally, agricultural pumps account for more than half of the total output of the pumps.

In the mining and metallurgical industries, mixed-flow pumps are also widely used. The mixed-flow pump is used for drainage and water supply in the process of beneficiation, smelting, and rolling in mines.

In the power sector, power stations need a large number of boiler feed pumps, condensate pumps, circulating pumps, and ash pumps, among which mixed-flow pumps account for the majority.

In the shipbuilding industry, many advanced water jet propulsion pumps are of mixed-flow pump types.

The following are examples of large-scale mixed-flow pump station projects in which Chinese companies have been engaged inside China as well as in neighboring countries for development of shipping, flood discharge, and other functions. The three representative projects are briefly described below:

1. Pumping station of Zaohe River in Suqian, Jiangsu province, China [2].
   The first-stage renovation project of the Zaohe River pumping station in the eastern route of the south-to-north water diversion project is located in Zaohe town, Suyu district, Suqian City, Jiangsu Province, China. Its primary task is to pump the diverted water from the Liulaodian pumping station into Luoma Lake, achieving a target water delivery of 175 m^3/s to Luoma Lake and addressing the drainage needs in the regions of Pihong River and Huangdun Lake.

   The Zaohe pumping station, shown in Fig. 1.3 is currently equipped with two sets of 5700HLQ100-4.78 vertical fully adjustable guide vane mixed-flow pumps. The pumps are designed with a net head of 4.78 meters, a design flow rate of 100 m^3/s, an impeller diameter of 5.70 meters, a rated speed of 75 r/min, and an adjustable blade angle in the range +2° to −18°. They are paired with TL7000-80/7400 vertical synchronous electric motors with a rated capacity of 7000 kW and a total installed capacity of 14 000 kW. The first unit was successfully started on April 8, 2011, at 15:40 in the afternoon.
2. Qushou pumping station of Qinglongshan irrigation area in Heilongjiang Sanjiang Plain, China [3].

Figure 1.3 Pumping station of Zaohe River in Suqian, Jiangsu province, China. Source: [2]. Jiangsu Aerospace Hydraulic Equipment Co., Ltd. https://www.pumpcj.com/case/95.html. Last accessed 17 January, 2024.

Figure 1.4 Qushou pumping station of Qinglongshan irrigation area in Heilongjiang Sanjiang Plain, China. Source: [3]. Jiangsu Aerospace Hydraulic Equipment Co., Ltd. https://www.pumpcj.com/case/97.html. Last accessed 17 January, 2024.

The installed flow rate capacity of the Qushou pumping station of Qinglongshan irrigation area is 381 m^3/s, and the total installed power capacity is 56 000 kW. It has six sets of 3300HLQ38.1-9.74 fully adjustable mixed-flow pumps to irrigate the largest irrigation area in Heilongjiang province. Furthermore, it is the second largest mixed-flow pump station in China, as shown in Fig. 1.4. This infrastructure plays a crucial role in realizing increased grain production and efficiency, optimizing the regional water resource allocation, and implementing the coordinated scheduling of surface water, groundwater, and rainwater resources for irrigation in the Sanjiang region – the largest granary in the country. It contributes significantly to promoting the coordinated and sustainable development of the economy, society, and ecology in the region.

3. The Belt and Road project of Chongqing Electromechanical Group – the Hyderabad flood control irrigation project in Telangana, India – has been successfully tested recently [4]. The 24 large, closed-volute mixed-flow pumps and 12 large synchronous motors used in the project have all been developed by Chongqing Hydro Turbine Co. Ltd. with independent intellectual property rights. Twenty-four large mixed-flow pumps are installed in this flood control and irrigation project. Each water pump has a flow of 41 m^3/s, a lift of 11 m, and a rotational speed of 136.6 r/min. It is the largest closed mixed-flow pump with single unit power of 6500 kW synchronous motor. The energy index and stability index of water pumps and synchronous motors have reached an international advanced level.

1.4 Summary

This chapter provides an overview of the main structural forms of the mixed-flow pump, its classifications, and industrial applications. In terms of the rotational speed, the specific speed (ns) ranges between 35 and 80 rpm for low-speed mixed-flow pumps and between 80 and 160 rpm for

higher-speed mixed-flow pumps. Considering the structure of the suction chamber, mixed-flow pumps can be categorized as volute mixed-flow pumps and guide vane mixed-flow pumps. Additionally, the broad applications of mixed-flow pumps in agricultural irrigation and other major industrial projects attest to their excellent operational range, performance, and stability.

References

1 https://www.ksb.com/centrifugal-pump-lexicon/mixed-flow-pump/192030.
2 https://www.pumpcj.com/case/95.html.
3 https://www.pumpcj.com/case/97.html.
4 https://rmh.pdnews.cn/Pc/ArtInfoApi/article?id=7493665.

2

Basic Concepts and Theory of Mixed-flow Pumps

2.1 Basic Flow and Performance Parameters

The parameters characterizing the performance of the pump are as follows.

2.1.1 Volume Flow *Q*

Flow is the volume (or mass) of liquid delivered in unit time. Volume flow is expressed in Q, the unit is m^3/s, m^3/h, or L/s, etc. The mass flow is expressed as Q_m and the unit is ton/h, kg/s, etc. The relationship between the mass flow and volume flow is

$$Q_m = \rho Q \tag{2.1}$$

where ρ is the density of the liquid in kg/m^3; ρ of clean water is generally taken as $1000\,kg/m^3$ at room temperature.

2.1.2 Head *H*

Head is the increment of energy per unit weight of liquid pumped by the pump from the pump inlet to the pump outlet. It is the effective energy obtained by 1 kg of liquid through the pump. The unit therefore is (N • m/N) = m, which is the equivalent liquid column height pumped by the pump shaft; the liquid column height is called the pump head H and is conventionally given in meters (m). The pump head can be written as

$$H = E_d - E_S \tag{2.2}$$

where E_d is energy per unit weight of liquid at the pump outlet in meters and E_s is energy per unit weight of liquid at the pump inlet in meters.

The energy per unit weight of the liquid is called head in hydraulics, which is usually composed of the pressure head $\frac{p}{\rho g}$ (m), the velocity head $\frac{v^2}{2g}$ (m), and the position head z (m), i.e.

$$E_d = \frac{p_d}{\rho g} + \frac{v_d^2}{2g} + z_d \tag{2.3}$$

and

$$E_s = \frac{p_s}{\rho g} + \frac{v_s^2}{2g} + z_s \tag{2.4}$$

Mixed-flow Pumps: Modeling, Simulation, and Measurements, First Edition.
Wei Li, Leilei Ji, Ramesh Agarwal, Weidong Shi, and Ling Zhou.

Therefore

$$H = \frac{p_d - p_s}{\rho g} + \frac{v_d^2 - v_s^2}{2g} + (z_d - z_s) \tag{2.5}$$

where p_d and p_s are the static pressure of the liquid at the pump outlet and inlet respectively, v_d and v_s are the liquid velocity at the pump outlet and inlet, respectively, and z_d and z_s are the distance from the pump outlet and inlet to a specified measuring datum plane respectively.

The head H of the pump is a key performance parameter of the pump, which is only related to the energy of the liquid at the inlet and outlet flanges of the pump and is not directly related to the type of the pump. However, using the energy equation, the pump head can be expressed by the energy of the liquid in the pump device.

2.1.3 Speed *n*

The speed n is the number of revolutions per unit time of the pump shaft, and its unit is revolutions r/min.

2.1.4 *NPSH*

The *NPSH*, an abbreviated form for the net positive suction head, is the main parameter indicating the cavitation performance of the pump. The *NPSH* has also been represented by Δh in the literature by some scientists.

2.1.5 Power and Efficiency

Pump power usually refers to the input power; it is the power transmitted by the prime mover to the pump shaft and is also known as the shaft power expressed by P.

The effective power of the pump, also known as the output power is expressed by P_e. It is the effective energy obtained by the liquid output from the pump per unit time.

Since the pump head is the effective energy obtained from the pump by the unit mass of liquid output from the pump, the product of head, mass flow, and gravity acceleration is the effective energy obtained from the liquid output from the pump in unit time, which is the effective power of the pump.

$$P_e = HQ_m g = \rho g Q H \text{ (Watt W)} \tag{2.6}$$

or

$$P_e = \frac{\rho g Q H}{1000} = \frac{\gamma Q H}{1000} \text{(kW)} \tag{2.7}$$

where ρ is the density of liquid delivered by the pump in kg/m^3, $\gamma = \rho g$ is the specific gravity of the liquid delivered by the pump in N/m^3, Q is the pump flow in m^3/s, H is the pump head in m, and g is the gravitational acceleration in m/s^2.

If the unit of specific gravity of the liquid is kg f/m^3, then

$$P_e = \frac{\gamma Q H}{100} \text{(kW)} \tag{2.8}$$

The difference in the shaft power P and the effective power P_e is the power loss in the pump, which is used to determine and define the efficiency of the pump. The efficiency of the pump is the ratio of the effective power to the shaft power expressed as

$$\eta = P_e / P \tag{2.9}$$

2.2 Typical Type of Flows in the Mixed-flow Pumps

2.2.1 Tip Leakage Flow

Since the tip leakage flow (TLF) in turbomachinery has significant impact on the performance and even safety of the machine, it is very important in the study of hydraulic machinery. Since the 1950s, the understanding of the TLF has been one of the major research topics in fluid mechanics of pumps, compressors, and turbines. The TLF model developed by Rains [1] is considered as the first original and seminal contribution which has served as a stepping stone toward the comprehensive understanding of this important flow phenomenon in turbomachines. Using this model, the velocity of TLF at the top of the outlet of the suction surface can be approximately estimated. At the same time, the change in the runner efficiency caused by TLF can be analyzed, but this model cannot calculate the micro-flow structure of the flow field. Later, Chen et al. [2] simplified the TLF model and deduced the trajectory coordinates of the two-dimensional tip leakage vortex (TLV) theoretically. Early experimental research and numerical simulations in the field of gas turbines provided a lot of information and data for exploring and analyzing the cause of formation as well as flow field structure of the flange leakage vortex [3, 4]. All these research efforts have enormously contributed to the present understanding of TLF and TLV.

Compared to the gas turbine, due to the large viscosity of water and more complex flow field in the end wall region, the research progress on TLF of the mixed-flow pump has been relatively slow. Yi et al. [5] employed the Reynolds-Averaged Navier-Stokes (RANS) equations with the SST k-ω turbulence model, revealing the formation mechanism of TLV and its influence on the performance of mixed-flow pump. Liu et al. [6] studied the shape and trajectory of the TLV in the mixed-flow pump, qualitatively and quantitatively analyzed the TLV, and determined that the TLV formed by the mixing of TLF and mainstream is the main reason for the deterioration of flow pattern and performance of the mixed-flow pump. Wu [7, 8], and Miorini et al. [9] used PIV technology to test and measure the flow field structure of TLV in the axial-flow water-jet propeller. It was found that the instantaneous TLV structure was formed by the unsteady vortex propagating to the top area of the blade channel, entraining with the mainstream and then breaking when reaching the pressure surface of adjacent blades. Using the PIV measurements, Masahiro et al. [10] tried to determine the generation mechanism of TLV of the mixed-flow pump at low flow rates and its impact in creating instability in the flow. It was found that the load on the impeller blade inlet rim increased with an increase in the leakage flow, and the TLV developed further with a decrease in the flow rate, forming a shroud of leakage flow.

Since TLF has a direct relationship with the clearance size, many researchers have studied the TLF under different tip clearances. Hah [11] and Li et al. [12] employed the LES to reveal the unsteady flow properties of TLF and TLV and analyzed the structure of TLF for five different tip clearances. Li et al. [13] studied the leakage flow for different tip clearances by performing numerical calculations and analyzed the formation and development process as well as the losses due to TLF and TLV for different tip clearances, and found that the strength of TLV increases with increase in tip clearance resulting in increase in losses. Zhang et al. [14] conducted the numerical simulation of a mixed-flow pump with low specific speed and analyzed its internal flow field for different tip clearances and found that the larger the tip clearance, the greater the effect of entrainment between the TLF and the mainstream flow. Goto [15] numerically analyzed the interaction mechanism of secondary flow and the formation mechanism of jet wake structure in the end wall region of the mixed-flow pump for four different tip clearances using the three-dimensional RANS equations and found that the reverse flow caused by the TLF at larger clearances is the main reason

for thickening of the boundary layer in the end wall region resulting in the deterioration of the entire flow field. Zhong et al. [16] studied the mixed-flow water-jet pump and analyzed the influence of different blade tip clearances on the performance and internal flow field of the water-jet pump and improved the blade profile in order to reduce the losses. Shi and Zhang [17, 18] studied the external flow characteristics as well as the internal flow field of the mixed-flow pump for different tip clearances through the combination of numerical simulation and experiment to analyze the evolution process of TLV and determine the influence of different tip clearances on formation and evolution of TLV and its effect on hydraulic performance and cavitation characteristics of the pump. Bing et al. [19] experimentally studied the efficiency drop of a mixed-flow pump ($\Delta\eta/\Delta\delta$) due to an increase in tip clearance $\Delta\delta$. It was found that the head, power, and efficiency decrease with an increase in tip clearance. A large number of studies have shown that TLF has a significant effect on the hydraulic performance of mixed-flow pumps. These studies provide a great deal of information toward the understanding of the complex three-dimensional flow field due to TLF in a mixed-flow pump.

2.2.2 Rotating Stall

The concept of the rotating stall in turbomachinery first appeared in 1955; it was first proposed by Emmons, [20] who provided a classical explanation as described in Fig. 2.1. Emmons considered an in-line cascade as an example to explain the rotating stall. The disturbances in the circumferential direction will easily occur due to the decrease of flow rate, and then resulting in an asymmetric flow. In addition, due to the uneven manufacturing or installation of blades, some flow channels in the impeller can generate separated flow, leading to stall and channel blockage. Assuming that blade C in Fig. 2.1 stalls first, flow separation will occur in the flow channel so that the flow in the flow channel between the adjacent blades D and C, opposite to the direction of rotation of the impeller, will be squeezed and the flow deformation shown in Fig. 2.1 will occur to avoid the extrusion area increasing the angle of attack of blade D and as a result the flow capacity in channel D will be weakened and the blockage in the flow channel will be exacerbated gradually entering into stall. The inlet angle of attack of adjacent blade B with the same direction of rotation as the impeller will decrease. If there is a stall in the flow channel of blade B, the blockage of the flow channel will be

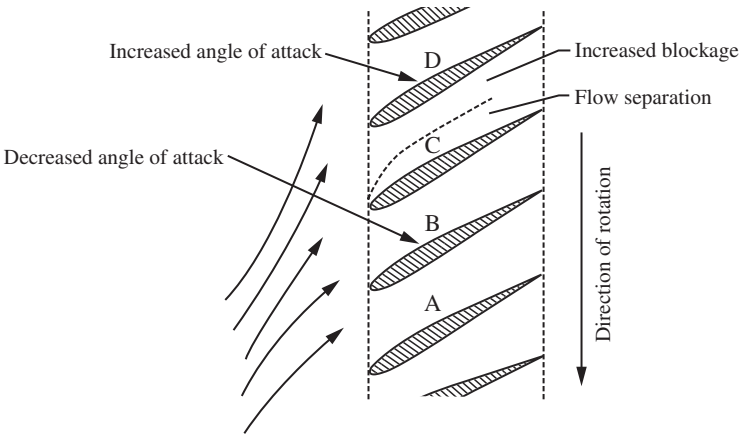

Figure 2.1 Diagram showing circumferential development of rotating stall. Source: Emmons et al. [20]/The American Society of Mechanical Engineers.